Research Article Vol. 10, No. 11 / November 2022 / Photonics Research 2575

PHOTONICS Research

Digitally tunable optical delay line based on thin-film lithium niobate featuring high switching speed and low optical loss

Wei Ke,[1] Yanmei Lin,[1] Mingbo He,[1] Mengyue Xu,[1] Jiaxiang Zhang,[2] Zhongjin Lin,[3,4] Siyuan Yu,[1] and Xinlun Cai[1,5]

[1]State Key Laboratory of Optoelectronic Materials and Technologies, School of Electronics and Information Technology, Sun Yat-sen University, Guangzhou 510275, China
[2]State Key Laboratory of Functional Materials for Informatics, Shanghai Institute of Microsystem and Information Technology, Chinese Academy of Sciences, Shanghai 200092, China
[3]Department of Electrical and Computer Engineering, The University of British Columbia, Vancouver, British Columbia V6T 1Z4, Canada
[4]e-mail: zlin23@ece.ubc.ca
[5]e-mail: caixlun5@mail.sysu.edu.cn

Received 26 July 2022; revised 28 August 2022; accepted 14 September 2022; posted 16 September 2022 (Doc. ID 471534); published 28 October 2022

A tunable optical delay line (ODL) featuring high switching speed and low optical loss is highly desirable in many fields. Here, based on the thin-film lithium niobate platform, we demonstrate a digitally tunable on-chip ODL that includes five Mach–Zehnder interferometer optical switches, four flip-chip photodetectors, and four delay-line waveguides. The proposed optical switches can achieve a switching speed of 13 ns and an extinction ratio of 34.9 dB. Using a modified Euler-bend-based spiral structure, the proposed delay-line waveguide can simultaneously achieve a small footprint and low optical propagation loss. The proposed ODL can provide a maximum delay time of 150 ps with a resolution of 10 ps and feature a maximum insertion loss of 3.4 dB.

https://doi.org/10.1364/PRJ.471534

1. INTRODUCTION

Optical delay lines (ODLs) have been applied in various fields, such as optical communication, microwave photonics, and optical coherence tomography [1–3]. For example, in optical signal processing, ODLs are used for feed-forward optical buffers and time-slot interchange units in future low-power-consumption and low-latency optical switching systems [4–6]. In microwave photonic systems, ODLs can be used as a key building block of microwave photonic beamformers in future compact size and large bandwidth radar systems [7–9]. To date, most commercial ODLs are still based on fiber-optic or free-space optical components [10–13] and generally require moving parts to achieve tunable operation; these parts are bulky in size, slow in response time, and cumbersome to use. Therefore, a tunable, compact, and low-cost ODL is highly desirable for integrated waveguide platforms.

In recent decades, several tunable ODLs based on different waveguide platforms have been proposed and experimentally demonstrated, such as silicon (Si), silicon nitride (Si_3N_4), silica, and polymers [14–21]. Most of the demonstrated tunable ODLs rely on the thermo-optic effect, resulting in a low switching speed and high power consumption. Using the plasma dispersion effect, a tunable ODL based on a silicon-on-insulator or indium phosphide can achieve nanosecond-level tuning speed. However, such a device suffers from high optical insertion loss and limited extinction ratio owing to free carrier absorption [22,23].

Recently, thin-film lithium niobate (TFLN) has emerged as an attractive material platform for high-performance photonic integrated devices [24]. For example, TFLN-based optical modulators with electro-optic (EO) bandwidths greater than 100 GHz and half-wave voltages of 1 V have been demonstrated [25–27]. TFLN-based polarization management devices have recently been demonstrated to simultaneously feature low optical loss, high-speed operation, compact size, and low drive voltage [28]. With the advantages of high-speed operation and low optical loss, TFLN is also an ideal material platform for realizing a high-performance tunable ODL. A TFLN-based tunable ODL has been reported previously with ultra-low loss delay waveguides; however, the fast electrical tuning operation of the ODL has not yet been demonstrated [29].

In this study, we propose a digitally 4-bit tunable ODL based on the TFLN platform comprising cascaded Mach–Zehnder interferometer (MZI) optical switches, flip-chip

bonded monitoring photodetectors (MPDs), and four delay-line waveguide spirals. This device can achieve a maximum delay time of 150 ps with a resolution of 10 ps. The insertion loss for the 150 ps delay time is 3.4 dB, corresponding to a delay loss of 0.023 dB/ps. The present device exhibits a switching speed of 13 ns between two arbitrary delays, which is the best value in the integrated tunable ODLs.

2. CONCEPT AND BUILDING BLOCKS

As shown in Fig. 1(a), the proposed device consists of five MZI optical switches, four delay-line waveguide spirals, four reference line waveguides, and four flip-chip bonded MPDs. The delay times of the four delay waveguides were 10, 20, 40, and 80 ps. The present device can provide a tunable delay time from 0 to 150 ps with a resolution of 10 ps by controlling the cross/bar states of the optical switches. Each reference line waveguide has a 1:99 directional coupler and a grating coupler. The outputs of the grating coupler are coupled to the flip-chip bonded MPDs, which are used to provide feedback on the cross/bar states of the optical switches. The device was designed and fabricated using an *X*-cut lithium niobate on insulator (LNOI) platform with a device layer thickness of 360 nm and buried oxide layer thickness of 4.7 μm. The waveguide was ridge-type with a height of 180 nm and a slab thickness of 180 nm. In the following, we discuss the details of the proposed optical switches and delay-line waveguide spirals.

TFLN-based 2 × 2 MZI optical switches are critical elements of the ODL device, as shown in Fig. 1(b). The optical splitters/combiners of the MZI were implemented using 2 × 2 3 dB multimode interferometer (MMI) couplers. The MZI operates in a single-drive push–pull configuration such that the electric fields induce phase shifts with an equal magnitude but opposite signs in the two arms. The arm length of the MZI was 2.5 mm. The gap between the electrodes and the width of the optical waveguide in between are 3.4 μm and 2 μm, respectively. The half-wave voltage of the device was measured as 10 V, corresponding to a length-voltage product of 2.5 V · cm. The extinction ratio of the MZI optical switch is measured to be as high as 34.9 dB, owing to the large fabrication tolerance of the MMI coupler. Moreover, the device exhibited an extinction ratio larger than 25 dB in the wavelength range of 1530–1575 nm [Fig. 1(d)]. High speed is one of the most prominent advantages of the TFLN-based optical switches. As shown in Fig. 1(e), the device can achieve a switching time of 13 ns, which is limited by the rising edge of the driving signal (1 MHz square wave). The proposed device does not experience the direct current (DC) bias draft [28,30].

A delay-line waveguide spiral is an important component. The spiral delay-line waveguide is composed of several bend and straight waveguides [Fig. 1(a)]. A modified Euler-bend multimode waveguide design was employed to reduce propagation loss [31–34]. The modified Euler-bend curve is defined as follows:

$$\frac{\mathrm{d}\theta}{\mathrm{d}L} = \frac{L}{A^2} + \frac{1}{R_{\max}}, \tag{1}$$

$$A = \left[L_0 \Big/ \left(\frac{1}{R_{\min}} - \frac{1}{R_{\max}}\right)\right]^{1/2}, \tag{2}$$

where L is the curve length from the start point and L_0 is the total length of the curve. $R_{\max}$ is the radius of the starting point, and $R_{\min}$ is the radius of the end point. $R_{\min}$ and $R_{\max}$ are

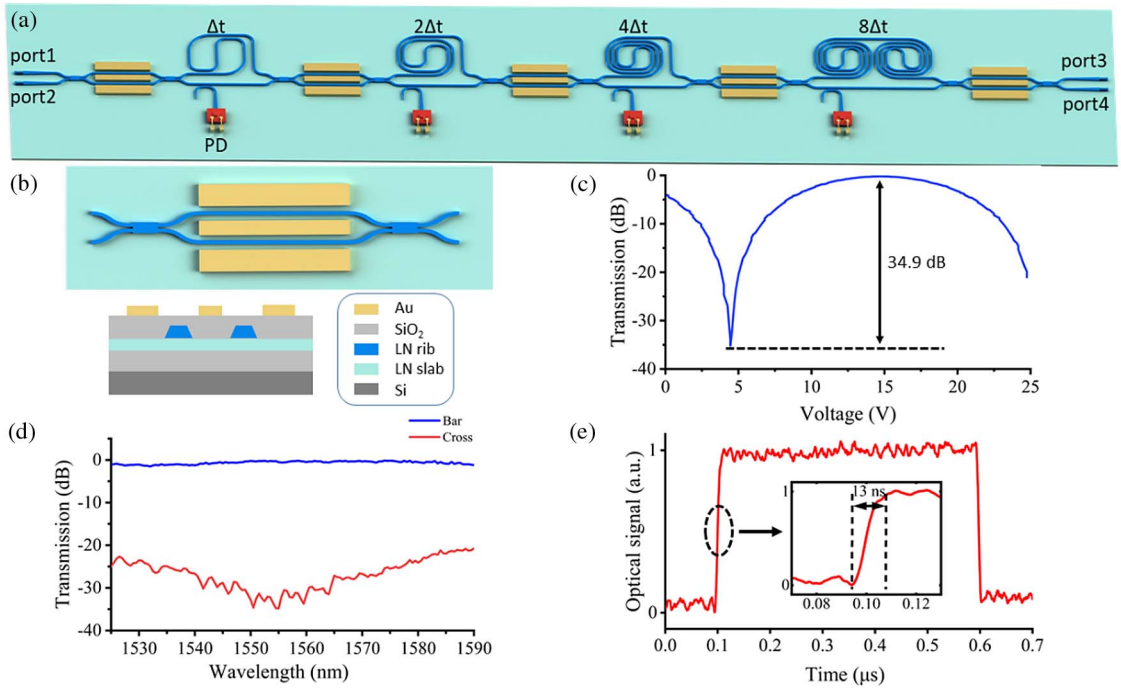

Fig. 1. (a) Schematic of the proposed 4-bit tunable optical delay line. PD, photodetector. (b) Architecture of 2 × 2 Mach–Zehnder interferometer (MZI) switch and its cross section. (c) Transmission spectrum of MZI switch with the applied voltage. (d) Transmission spectrum of MZI switch at bar/cross states. (e) Fast-switching spectrum of MZI when applied a 1 MHz square wave.

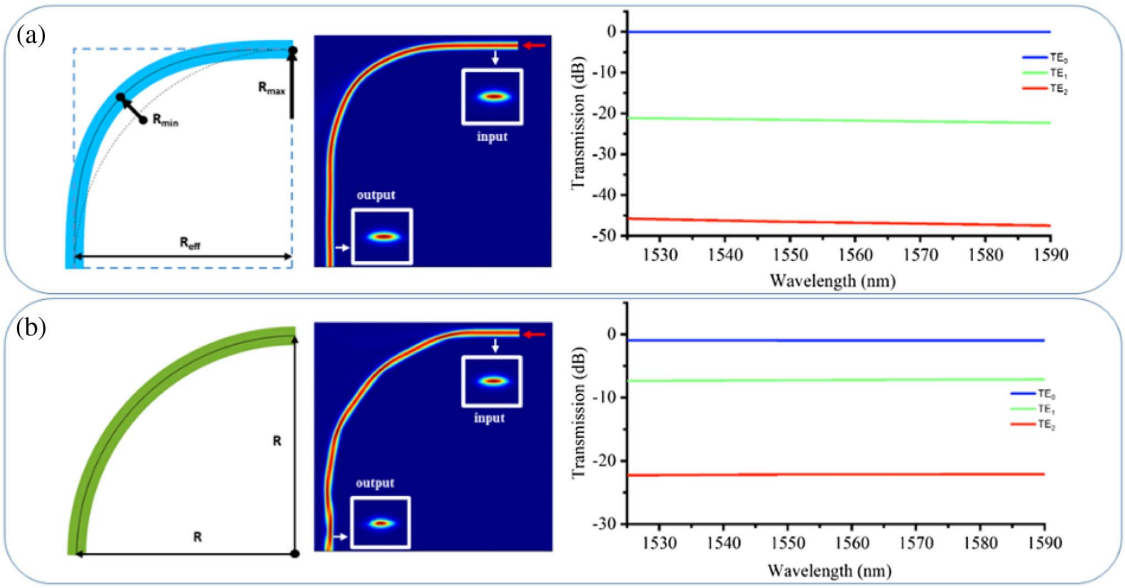

Fig. 2. Comparison of arc bend and modified Euler bend. The schematics and corresponding simulation results of (a) modified Euler-bend waveguide and (b) regular arc bend waveguide with the same radius of 46 μm and width of 2.2 μm, respectively.

designed such that no high-order modes are excited when light propagates in the bend waveguide.

Figure 2 shows a comparison of the regular arc bend and modified Euler-bend waveguides. Both the regular arc bend and modified Euler-bend waveguides were simulated with the same footprint of 46 μm × 46 μm and a width of 2.2 μm. Figure 2(a) indicates that when injecting a fundamental transverse electric field (TE_0) with a wavelength of 1550 nm, the TE_0 mode propagates smoothly in the 90° modified Euler-bend waveguide, and no notable inter-mode is observed. Moreover, the corresponding transmission spectrum shows that the high-order modes excited in the modified Euler-bend waveguide are lower than −22 dB. In contrast, a significant multimode inference occurred in the regular arc-bend waveguide [Fig. 2(b)].

Based on the wide waveguides and modified Euler bend, the delay-line waveguide spirals can simultaneously achieve low loss and compactness. The distance between two adjacent waveguides was set to 10 μm, sufficient to avoid evanescent coupling. In this case, waveguide spirals with lengths greater than 1.57 cm can be placed in an area of 500 μm × 500 μm. Since the widths of waveguides in the optical switches and delay-line waveguide spirals are different, they are connected with MMI couplers through different tapers.

3. FABRICATION AND EXPERIMENTS

The fabrication process is detailed in the Appendix A. Figure 3(a) presents a microscopy image of the fabricated tunable ODL, and the inset of Fig. 3(a) presents a magnified image of one MZI switch. The footprint of the fabricated device is 25 mm × 2 mm. Figures 3(b) and 3(c) present the microscopy images of the flip-chip MPDs and modified Euler-bend-based waveguide spiral, respectively. As discussed in Appendix B, the average group index of the waveguide spiral is 2.245. Therefore, the total length of the delay-line waveguide of the proposed device is 2 cm.

A. Characterization of Delay Time

A schematic of the experimental setup used for measuring the delay time of the ODL is shown in Fig. 4(a). The delay time can be obtained by comparing the output microwave signal generated by the vector network analyzer (VNA) and its local replica. In the experiment, the wavelength of the tunable laser was set as 1550 nm. More details about the experiment, including the calibration of the voltage applied to each optical switch, can be found in Appendix C.

We applied combinations of voltages to the tunable ODL to generate six different delay times, ranging from 0 to 150 ps [Fig. 4(b)]. Figure 4(c) shows the measured delay times, consistent with the expected values. The optical losses of the fabricated device for different delay times are shown in Fig. 4(d). The maximum and minimum on-chip insertion losses of the tunable ODL were 3.4 dB and 2.5 dB, respectively. The on-chip loss for 3.4 dB can be broken down as follows: the losses for the delay-line waveguides and five optical switches are 0.9 dB and 2.5 dB, respectively. The insertion loss of the proposed device can be further decreased after improving the fabricated processing.

B. High-Speed Tunability Experiment

To demonstrate the performance of high-speed tunability, the delay time of our device was switched between 100 and 150 ps and between 20 and 150 ps, respectively [Figs. 5(a) and 5(b)]. Four square-wave electrical signals with a repetition rate of 125 kHz and a sampling rate of 2 MHz, generated from the multifunction I/O module (NI PXIe-6363), were simultaneously applied to the four optical switches, while a constant electrical signal was applied to the remaining optical switch. The output optical powers are presented at the bottom of

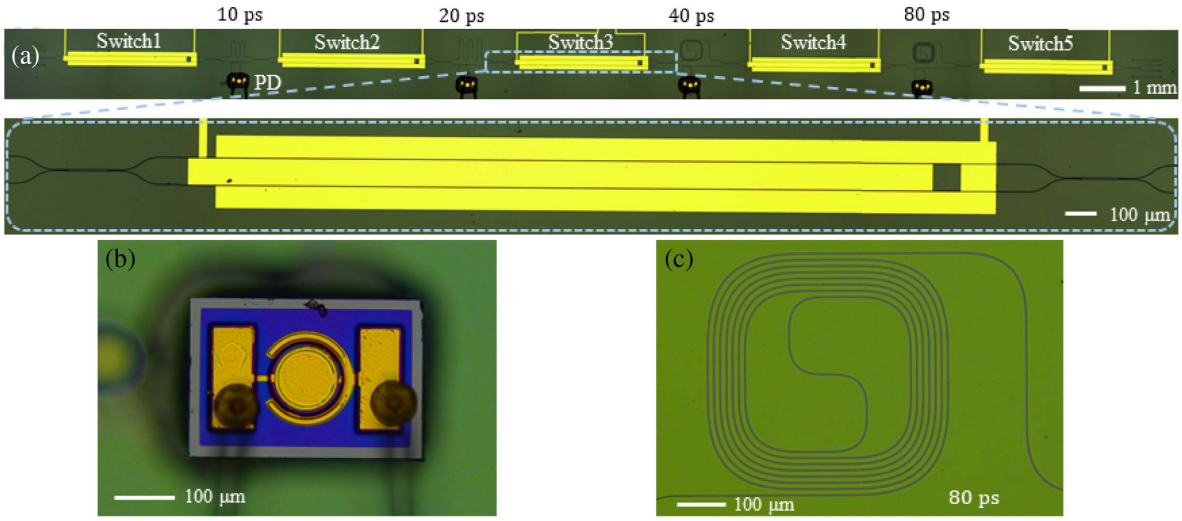

Fig. 3. (a) Microscopy image of the fabricated device and one of the MZI switches. Microscopy of (b) back-sensing on-chip photodiode and (c) delay-line waveguide spiral with a delay of 80 ps used in the proposed device, respectively.

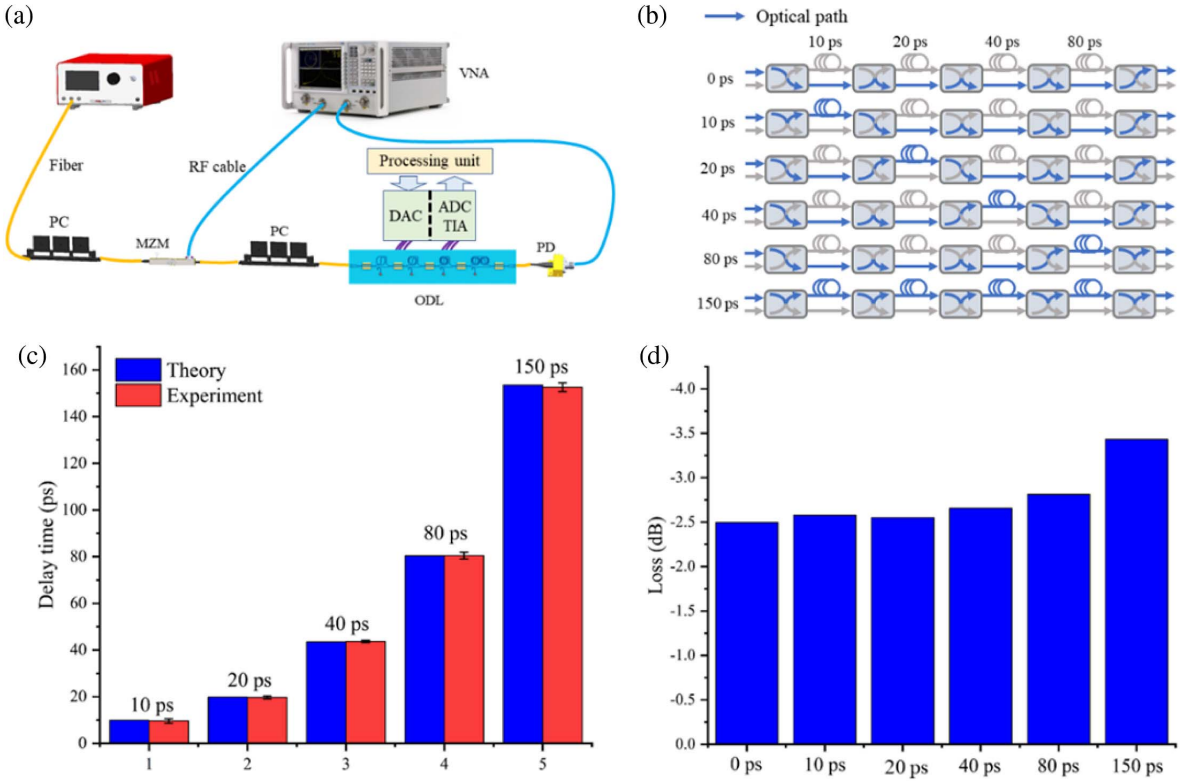

Fig. 4. (a) Experimental setup for optical delay characterization. PC, polarization controller; MZM, Mach–Zehnder modulator; ADC/DAC, analog-to-digital converter/digital-to-analog converter; TIA, trans-impedance amplifier; ODL, optical delay line; PD, photodetector; VNA, vertical network analyzer. (b) Schematic of the optical path for different delay times. (c) Comparison between theoretical and measured delay times. (d) Optical insertion loss for different delay times.

Figs. 5(a) and 5(b), indicating that the switching time of the fabricated ODL can achieve 0.5 μs. The switching speed of the proposed ODL is limited by the speed of the electrical control system. Using a higher-speed electrical control system, the switching time of the fabricated ODL can be further improved to be close to 13 ns. (Details can be found in Appendix D.) In theory, the switching time of the proposed tunable ODL is equal to the sum of maximum delay time and switching time of the single optical switch as discussed in Appendix E.

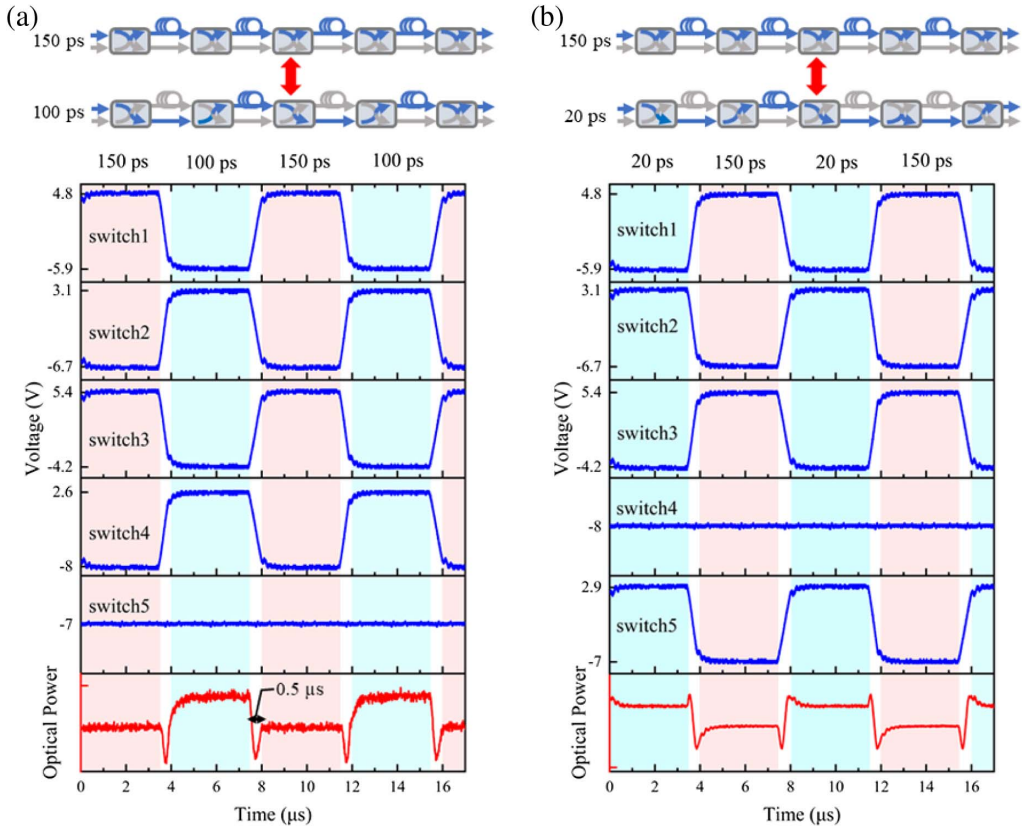

Fig. 5. (a) and (b) show the schematics of the optical paths and the corresponding transmission optical power when the delay time is tuned between 150 and 100 ps and between 150 and 20 ps, respectively.

4. CONCLUSIONS

Based on the TFLN platform, a tunable ODL with a maximum delay time of 150 ps and a resolution of 10 ps was proposed and experimentally demonstrated. The proposed optical switch exhibits a switching speed of 13 ns and an extinction ratio of 34.9 dB, which outperforms other tunable ODLs as shown in Table 1. Moreover, using the modified Euler bends to build the delay-line waveguide, the maximum optical insertion loss of the proposed tunable ODL is only 3.4 dB. With its advantages of low optical loss and fast switching speed, the proposed device has significant potential in optical communication, microwave photonics, optical autocorrelators, and optical coherence tomography applications.

APPENDIX A: FABRICATION OF THE PROPOSED DEVICE

The fabrication process of the proposed device is shown in Fig. 6. The device was fabricated in an *X*-cut LNOI wafer (NANOLN), which consists of an LN layer with a thickness of 360 nm and a buried oxide (SiO_2) layer with a thickness of 4.7 μm. First, all structures including waveguides, multimode interference (MMI) couplers, and grating couplers were defined by e-beam lithography (EBL) and etched by inductively coupled plasma (ICP) [see Figs. 6(a)–6(e)]. Then, silicon dioxide with a thickness of 1 μm was deposited on the top of the chip [see Fig. 6(f)]. Finally, we used EBL and e-beam evaporation (EBE) to transfer and produce the patterns of electrodes

Table 1. Comparison of Various Switchable Delay Lines

	Material	Delay Range (ps)	Resolution (ps)	Delay Loss (dB/ps)	Power Efficiency (mW/ps)	Switching Time[a] (μs)	Footprint (mm^2)
7-bit ODL [7]	SOI	191.37	1.42	0.1	1.26	33.7	22.23
7-bit ODL[b] [14]	SOI	1270	10	0.009	0.05	18.97	28.62
4-bit ODL [18]	Si_3N_4/SiO_2	12,350	850	0.001	0.02	-	3825
4-bit ODL [21]	Polymer	177	11.8	0.084	0.8	2800	297
4-bit ODL [35]	Silica	90.2	6	0.026	1.47	840	602
Our work	TFLN	150	10	0.023	Negligible[c]	0.013	50

[a]The switching time of other ODLs is the switching time of a single switch.
[b]Only switchable delay line is in consideration.
[c]Our device only consumes power when driving voltages are changing.

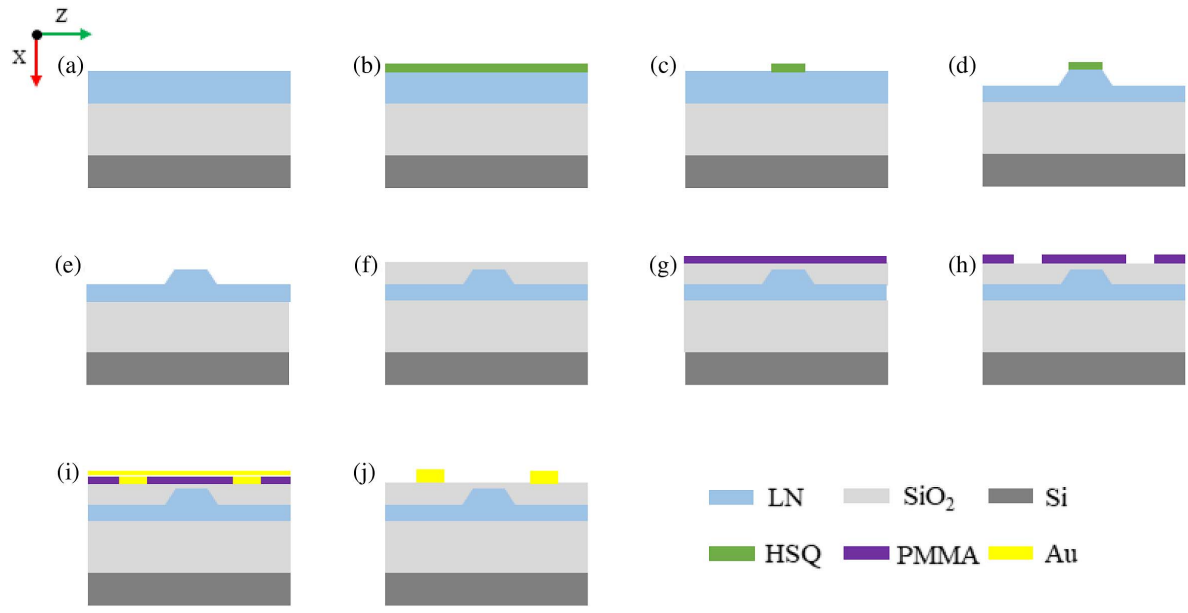

Fig. 6. Fabrication flow of the proposed optical delay line. HSQ, hydrogen silsesquioxane; PMMA, polymethylmethacrylate.

onto the chip [see Figs. 6(g)–6(i)]. The material and thickness of the fabricated electrodes are gold and 900 nm. A lift-off process was performed to produce the gold electrode [see Fig. 6(j)].

APPENDIX B: GROUP INDEX OF WAVEGUIDE SPIRAL

The effective index of the waveguide in the y direction and z direction varying with the wavelength is shown in Fig. 7(a). The group index of the waveguide in the y and z directions is 2.19 and 2.29, respectively. Through measuring the delay time of the fabricated delay-line waveguide spirals, which have different lengths [see Fig. 7(b)], we can know that the average group index of the waveguide is measured to be 2.245. In the proposed tunable ODL, the total length of all delay-line waveguides is 2 cm.

APPENDIX C: DETAILS OF THE CHARACTERIZATION OF DELAY

The measurement setup is shown in Fig. 4(a). A microwave signal with 10 GHz from vector network analyzer (VNA) was modulated on a commercial Mach–Zehnder Modulator (MZM). Then, the optical signal passed through the device through different paths and was injected into the MPD, which converted the optical signal to a microwave signal back into VNA. The VNA received the microwave signal and retrieved the phase responses of the microwave signal by comparing

Table 2. Switching Voltages of Switches (in V)

	Switch1	Switch2	Switch3	Switch4	Switch5
Bar	4.8	–6.7	5.4	–8	–7
Cross	–5.9	3.1	–4.2	2.6	2.9

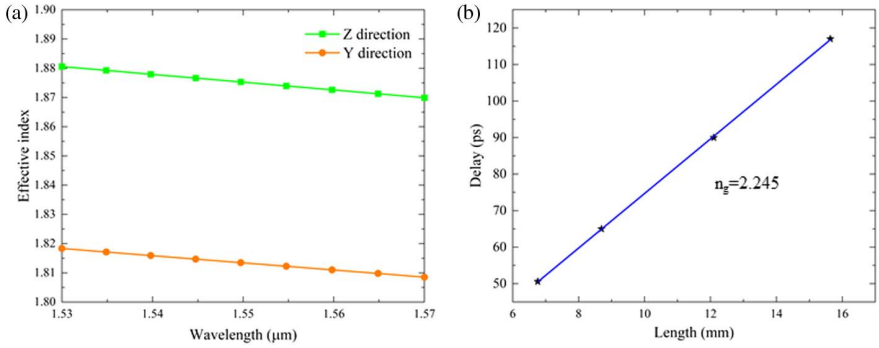

Fig. 7. (a) Simulated effective index of the waveguide in the y direction and z direction varying with wavelength. (b) Measured delay time of the fabricated waveguide spirals with different lengths.

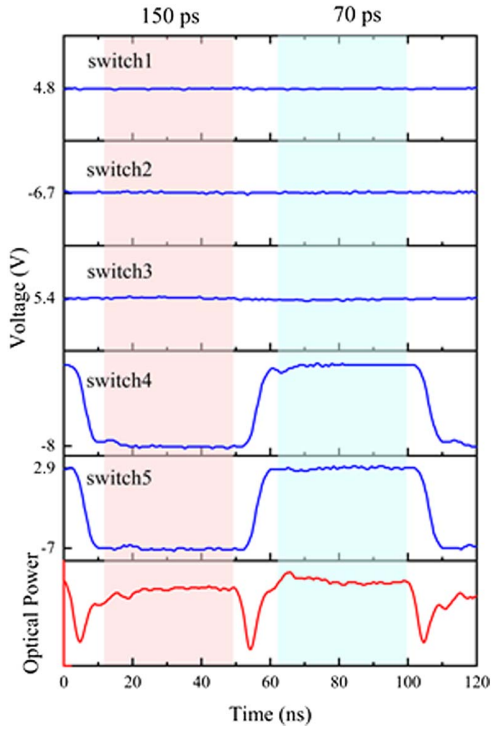

Fig. 8. Two square waves applied to the switches and corresponding transmission optical power.

the input signal and its local replica. The time delay can be obtained from the derivate of phase to regular frequency.

First, we calibrated the bias voltage of the device. In principle, the initial state of a single switch should be at the cross state. However, the bias voltage required for each switch to reach the initial state needs to be calibrated due to fabrication imperfection. The PXI multifunction I/O module can not only be used as a multichannel voltage source to drive the optical switches of device, but also read the output voltages of the flip-chip bonded MPD. We wrote a program on LabVIEW to display the real-time input and output voltage of the PXI multifunction I/O module. According to the optical power feedback from the flip-chip MPD, we confirmed the switching voltage of switches one by one as shown in Table 2. Then, the delay of the fabricated device can be tuned by controlling the voltage applied to the five optical switches.

APPENDIX D: HIGH-SPEED TUNABILITY EXPERIMENT

With the limitation of our experiment setup, we cannot simultaneously generate four square waves with high repetition rate and high amplitude. Therefore, to show the shortest switching time of our device, we used a two-channel arbitrary waveform generator to control two switches, while the other three remained bar state constant. As shown in Fig. 8, when the repetition rate of the square waves applied to the switches increased to 10 MHz, the switching time of the fabricated ODL decreased to near 13 ns.

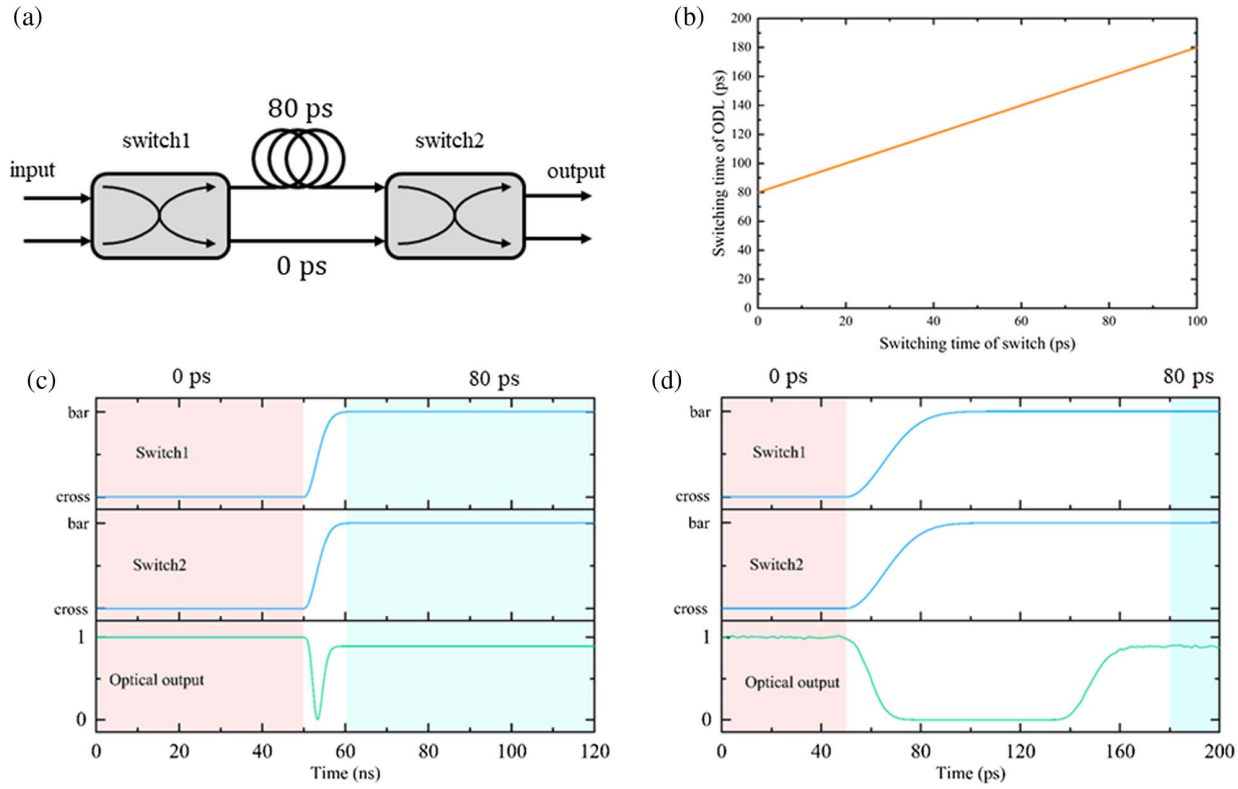

Fig. 9. (a) Schematic of a 1-bit tunable optical delay line (ODL). (b) Switching time of ODL varying with the switching time of the single switch. (c), (d) Simulation results when switching time of switch is set at 10 ns and 50 ps, respectively.

APPENDIX E: THEORETICAL SHORTEST SWITCHING TIME OF THE PROPOSED ODL

In theory, the switching time of the proposed tunable ODL is equal to the sum of the maximum delay time and the switching time of the single optical switch. To demonstrate this, as shown in Fig. 9(a), we built a model of a 1-bit tunable ODL using Interconnect (Lumerical Inc.). Figure 9(b) presents the numerical results of the switching time of the ODL varying with that of the optical switch. Figures 9(c) and 9(d) present the cases in which the switching time of the switch was set at 10 ns and 50 ps, respectively.

Funding. National Key Research and Development Program of China (2019YFA0705004, 2019YFB1803901); Key R&D Program of Guangdong Province (2018B03032900); Local Innovative and Research Teams Project of Guangdong Pearl River Talents Program (2017BT01X121).

Acknowledgment. We thank Lidan Zhou, Lin Liu, and Shengqian Gao for their technical support.

Disclosures. The authors declare no conflicts of interest.

Data Availability. No data were generated or analyzed in the presented research.

REFERENCES

1. D. Gauthier, "Slow light brings faster communications," Phys. World **18**, 30–32 (2005).
2. J. T. Mok and B. J. Eggleton, "Photonics: expect more delays," Nature **433**, 811–812 (2005).
3. L. Zhou, X. Wang, L. Lu, and J. Chen, "Integrated optical delay lines: a review and perspective [Invited]," Chin. Opt. Lett. **16**, 101301 (2018).
4. R. S. Tucker, P.-C. Ku, and C. J. Chang-Hasnain, "Slow-light optical buffers: capabilities and fundamental limitations," J. Lightwave Technol. **23**, 4046–4066 (2005).
5. Z. Wang, N. Chi, and S. Yu, "Time-slot interchange using an optical buffer with a large variable delay range based on an active-vertical-coupler crosspoint switch," Opt. Eng. **45**, 105003 (2006).
6. M. Moralis-Pegios, G. Mourgias-Alexandris, N. Terzenidis, M. Cherchi, M. Harjanne, T. Aalto, A. Miliou, N. Pleros, and K. Vyrsokinos, "On-chip SOI delay line bank for optical buffers and time slot interchangers," IEEE Photon. Technol. Lett. **30**, 31–34 (2018).
7. P. Zheng, C. Wang, X. Xu, J. Li, D. Lin, G. Hu, R. Zhang, B. Yun, and Y. Cui, "A seven bit silicon optical true time delay line for Ka-band phased array antenna," IEEE Photon. J. **11**, 5501809 (2019).
8. C. Zhu, L. Lu, W. Shan, W. Xu, G. Zhou, L. Zhou, and J. Chen, "Silicon integrated microwave photonic beamformer," Optica **7**, 1162–1170 (2020).
9. P. Zheng, X. Xu, D. Lin, P. Liu, G. Hu, B. Yun, and Y. Cui, "A wideband 1 × 4 optical beam-forming chip based on switchable optical delay lines for Ka-band phased array," Opt. Commun. **488**, 126842 (2021).
10. S. Li, X. Li, W. Zou, and J. Chen, "Rangeability extension of fiber-optic low-coherence measurement based on cascaded multistage fiber delay line," Appl. Opt. **51**, 771–775 (2012).
11. S. Granieri, M. Jaeger, and A. Siahmakoun, "Multiple-beam fiber-optic beamformer with binary array of delay lines," J. Lightwave Technol. **21**, 3262–3272 (2003).
12. E. Choi, J. Na, S. Y. Ryu, G. Mudhana, and B. H. Lee, "All-fiber variable optical delay line for applications in optical coherence tomography: feasibility study for a novel delay line," Opt. Express **13**, 1334–1345 (2005).
13. M. Yessenov and A. F. Abouraddy, "Demonstration of a free-space optical delay line using space-time wave packets," in *Frontiers in Optics + Laser Science APS/DLS*, OSA technical digest (Optica Publishing Group, 2019), paper FW1C.1.
14. X. Wang, L. Zhou, R. Li, J. Xie, L. Lu, K. Wu, and J. Chen, "Continuously tunable ultra-thin silicon waveguide optical delay line," Optica **4**, 507–515 (2017).
15. Y. Wang, H. Sun, M. Khalil, W. Dong, I. Gasulla, J. Capmany, and L. R. Chen, "On-chip optical true time delay lines based on subwavelength grating waveguides," Opt. Lett. **46**, 1405–1408 (2021).
16. J. Xie, L. Zhou, Z. Li, J. Wang, and J. Chen, "Seven-bit reconfigurable optical true time delay line based on silicon integration," Opt. Express **22**, 22707–22715 (2014).
17. Z. Ke, R. Ge, and X. Cai, "Tunable optical true time delay line based on ring array," in *Asia Communications and Photonics Conference (ACP)*, OSA technical digest (Optica Publishing Group, 2018), paper S3F.4.
18. R. L. Moreira, J. Garcia, W. Li, J. Bauters, J. S. Barton, M. J. R. Heck, J. E. Bowers, and D. J. Blumenthal, "Integrated ultra-low-loss 4-bit tunable delay for broadband phased array antenna applications," IEEE Photon. Technol. Lett. **25**, 1165–1168 (2013).
19. K. Horikawa, I. Ogawa, H. Ogawa, and T. Kitoh, "Photonic switched true time delay beam forming network integrated on silica waveguide circuits," in *Proceedings of 1995 IEEE MTT-S International Microwave Symposium* (1995), Vol. **61**, pp. 65–68.
20. M. S. Rasras, J. L. Grange, C. K. Madsen, M. A. Cappuzzo, E. Chen, L. Gomez, E. J. Laskowski, A. Griffin, A. Wong-Foy, A. Kasper, and S. S. Patel, "Integrated scalable continuously tunable variable optical delay lines," in *IEEE LEOS Annual Meeting Conference Proceedings* (2005), pp. 736–737.
21. X. Wang, B. Howley, M. Y. Chen, and R. T. Chen, "Phase error corrected 4-bit true time delay module using a cascaded 2 × 2 polymer waveguide switch array," Appl. Opt. **46**, 379–383 (2007).
22. D. Thomson, A. Zilkie, J. E. Bowers, T. Komljenovic, G. T. Reed, L. Vivien, D. Marris-Morini, E. Cassan, L. Virot, J.-M. Fédéli, J.-M. Hartmann, J. H. Schmid, D.-X. Xu, F. Boeuf, P. O'Brien, G. Z. Mashanovich, and M. Nedeljkovic, "Roadmap on silicon photonics," J. Opt. **18**, 073003 (2016).
23. M. Li, L. Wang, X. Li, X. Xiao, and S. J. P. R. Yu, "Silicon intensity Mach–Zehnder modulator for single lane 100 Gb/s applications," Photon. Res. **6**, 109–116 (2018).
24. D. Zhu, L. Shao, M. Yu, R. Cheng, B. Desiatov, C. J. Xin, Y. Hu, J. Holzgrafe, S. R. Ghosh, A. Shams-Ansari, E. Puma, N. Sinclair, C. Reimer, M. Zhang, and L. Marko, "Integrated photonics on thin-film lithium niobate," Adv. Opt. Photon. **13**, 242–352 (2021).
25. C. Wang, M. Zhang, X. Chen, M. Bertrand, A. Shams-Ansari, S. Chandrasekhar, P. Winzer, and M. Lončar, "Integrated lithium niobate electro-optic modulators operating at CMOS-compatible voltages," Nature **562**, 101–104 (2018).
26. M. Xu, M. He, H. Zhang, J. Jian, Y. Pan, X. Liu, L. Chen, X. Meng, H. Chen, Z. Li, X. Xiao, S. Yu, S. Yu, and X. Cai, "High-performance coherent optical modulators based on thin-film lithium niobate platform," Nat. Commun. **11**, 3911 (2020).
27. B. Pan, H. Cao, Y. Huang, Z. Wang, K. Chen, H. Li, Z. Yu, and D. Dai, "Compact electro-optic modulator on lithium niobate," Photon. Res. **10**, 697–702 (2022).
28. Z. Lin, Y. Lin, H. Li, M. Xu, M. He, W. Ke, H. Tan, Y. Han, Z. Li, D. Wang, X. S. Yao, S. Fu, S. Yu, and X. Cai, "High-performance polarization management devices based on thin-film lithium niobate," Light Sci. Appl. **11**, 93 (2022).
29. J.-X. Zhou, R.-H. Gao, J. Lin, M. Wang, W. Chu, W.-B. Li, D.-F. Yin, L. Deng, Z.-W. Fang, J.-H. Zhang, R.-B. Wu, and Y. Cheng, "Electro-optically switchable optical true delay lines of meter-scale lengths fabricated on lithium niobate on insulator using photolithography assisted chemo-mechanical etching," Chin. Phys. Lett. **37**, 084201 (2020).
30. Y. Pan, M. He, M. Xu, Z. Lin, Y. Lin, W. Ke, J. Liu, Z. Lin, Y. Zhu, S. Gao, H. Li, X. Liu, C. Liu, S. Yu, and X. Cai, "Compact

substrate-removed thin-film lithium niobate electro-optic modulator featuring polarization-insensitive operation," Opt. Lett. **47**, 1818–1821 (2022).
31. M. Bahadori, M. Nikdast, Q. Cheng, and K. Bergman, "Universal design of waveguide bends in silicon-on-insulator photonics platform," J. Lightwave Technol. **37**, 3044–3054 (2019).
32. X. Jiang, H. Wu, and D. Dai, "Low-loss and low-crosstalk multimode waveguide bend on silicon," Opt. Express **26**, 17680–17689 (2018).
33. L. H. Gabrielli, D. Liu, S. G. Johnson, and M. Lipson, "On-chip transformation optics for multimode waveguide bends," Nat. Commun. **3**, 1217 (2012).
34. D. Dai, "Multimode optical waveguide enabling microbends with low inter-mode crosstalk for mode-multiplexed optical interconnects," Opt. Express **22**, 27524–27534 (2014).
35. Q. Song, Z. Hu, and K. Chen, "Scalable and reconfigurable true time delay line based on an ultra-low-loss silica waveguide," Appl. Opt. **57**, 4434–4439 (2018).